

Riemannian Perspective on Matrix Factorization

Kwangjun Ahn^{*1} and Felipe Suarez^{†2}

¹Department of Electrical Engineering and Computer Science, MIT

²Department of Mathematics, MIT

Abstract

We study the non-convex matrix factorization approach to matrix completion via Riemannian geometry. Based on an optimization formulation over a Grassmannian manifold, we characterize the landscape based on the notion of principal angles between subspaces. For the fully observed case, our results show that there is a region in which the cost is geodesically convex, and outside of which all critical points are strictly saddle. We empirically study the partially observed case based on our findings.

1 Introduction

Matrix completion is a classical problem in machine learning and signal processing that aims to recover an unknown low-rank matrix from only a few observed entries. Ever since the pioneering work by [Candès and Recht \(2009\)](#), there have been a flurry of works solving matrix completion with guarantees. See a survey by [Candès and Recht \(2012\)](#) and the introduction of [\(Ge et al., 2016\)](#) for detailed information.

Among many approaches, one prominent approach widely used in practice is based on matrix factorizations, *à la* [Burer and Monteiro \(2003\)](#). Letting M be the $m \times n$ unknown matrix of rank r , the matrix factorization approach solves

$$\underset{\substack{\mathbf{X} \in \mathbb{R}^{m \times r} \\ \mathbf{Y} \in \mathbb{R}^{n \times r}}}{\text{minimize}} \frac{1}{2} \sum_{(i,j): \text{observed}} [(\mathbf{XY}^\top)_{i,j} - \mathbf{M}_{i,j}]^2. \quad (1.1)$$

Due to explicit factorization, the matrix factorization approach is computationally advantageous, making it widely applicable in practice ([Koren, 2009](#)).

^{*}Email: kjahn@mit.edu. This work was supported by graduate assistantship from the NSF Grant (CA-REER: 1846088) and by Kwanjeong Educational Foundation.

[†]Email: felipesc@mit.edu. This work was supported in part by a graduate assistantship from the NSF award IIS-1838071.

To complement its success in practice, there have been a great number of works trying to understand the matrix factorization approach *theoretically* (Keshavan et al., 2010; Jain et al., 2013; Hardt, 2014; Hardt and Wotter, 2014; Sun and Luo, 2016; Zhao et al., 2015; Chen and Wainwright, 2015; De Sa et al., 2015; Ge et al., 2016; Bhojanapalli et al., 2016; Ge et al., 2017; Park et al., 2017). As discussed in the seminal work by Sun and Luo (2016), the main difficulty lies in the non-convex nature of the problem, arising from the problem symmetry. For instance, if a pair $(\mathbf{X}^*, \mathbf{Y}^*)$ achieves the global optimum of (1.1), then it follows from the symmetry that $(\mathbf{X}^* \mathbf{R}, \mathbf{Y}^* (\mathbf{R}^{-1})^\top)$ for any invertible \mathbf{R} also achieves the optimum. In particular, the non-convexity of matrix factorization eludes conventional theoretical frameworks based on convex analysis.

In this work, we study the matrix factorization approach from a Riemannian geometric perspective. Inspired by previous works (Dai et al., 2011; Boumal and Absil, 2011; Dai et al., 2012; Boumal and Absil, 2015; Pitaval et al., 2015), we consider a formulation of the matrix factorization approach as an optimization over a single Grassmannian. We then investigate the Riemannian geometry of the cost function. For the fully observed case, our main result offers a crisp characterization of the landscape based on the notion of principal angles between subspaces. More specifically, our result characterizes a region in which the cost function is geodesically convex and outside of which the cost function has an escaping direction, i.e. a direction along which the second derivative is negative. In particular, all critical points outside this region are strictly saddle. Lastly, we empirically study the partially observed case and observe that the landscape resembles the fully observed case for the settings considered in previous works.

1.1 Related work

Over the last decade, there have been a myriad of works solving matrix completion via *Riemannian optimization*¹ (Edelman et al., 1998; Absil et al., 2004). Previous methodological contributions have employed various optimization methods, such as (stochastic) gradient descent (Keshavan and Oh, 2009; Keshavan et al., 2010; Balzano et al., 2010; Mishra et al., 2012, 2014), conjugate gradient methods (Vandereycken, 2013; Boumal and Absil, 2011; Mishra et al., 2012; Boumal and Absil, 2015; Cambier and Absil, 2016), trust-region methods (Boumal and Absil, 2011; Mishra et al., 2012, 2014; Boumal and Absil, 2015), Newton’s method (Simonsson and Eldén, 2010), scaled gradient methods (Ngo and Saad, 2012), and others. Only a few works have studied the theoretical aspect of the Riemannian optimization approach. The closest result to ours can be found in (Pitaval et al., 2015) where they show the global convergence of a Riemannian gradient flow. Another related result can be found in (Keshavan et al., 2010, §6) where they study *local* geometry of their formulation based on *two* Grassmannian manifolds. Other works study formulations based on *different* manifolds. For instance, (Wei et al., 2016) and (Hou et al., 2020) study the formulation based on the manifold of fixed rank matrices.

¹See a recent monograph (Boumal, 2020) for a gentle introduction on optimization over Riemannian manifolds.

Apart from matrix completion, over the last few years, there have been many works understanding Riemannian landscape for other problems, including dictionary learning (Sun et al., 2016; Bai et al., 2018; Zhu et al., 2019; Li et al., 2019), (robust) subspace recovery (Maunu et al., 2019; Zhu et al., 2019; Li et al., 2019), matrix sensing (Hou et al., 2020), and point-set registration (Bohorquez et al., 2020).

1.2 Setting and notations

Setting. We use bold lower-case letters (e.g. $\mathbf{u}, \mathbf{v}, \mathbf{x}, \mathbf{y}$) to denote vectors, and bold upper-case letters (e.g. $\mathbf{U}, \mathbf{V}, \mathbf{X}, \mathbf{Y}$) to denote matrices, and reserve \mathbf{O} for the zero matrix. We assume that the ground truth matrix \mathbf{M} is a $m \times n$ matrix ($m \leq n$) of rank r whose singular value decomposition is $\mathbf{U}\Sigma\mathbf{V}^\top$. Let σ_{\min} and σ_{\max} be the smallest and largest singular value, respectively. Let $\Omega \subset [m] \times [n]$ be the subset of observed positions. For $\mathbf{A} \in \mathbb{R}^{m \times n}$, \mathbf{A}_Ω is the $m \times n$ matrix defined as $(\mathbf{A}_\Omega)_{i,j} = \mathbf{A}_{i,j}$ if $(i, j) \in \Omega$ and $(\mathbf{A}_\Omega)_{i,j} = 0$ otherwise. $\langle \mathbf{A}, \mathbf{B} \rangle_\Omega$ denotes the inner product $\text{Tr}[(\mathbf{A}_\Omega)^\top \mathbf{B}_\Omega]$ and $\|\mathbf{A}\|_\Omega^2 := \langle \mathbf{A}, \mathbf{A} \rangle_\Omega$.

Other notations. The column space is denoted $\text{col}(\cdot)$. The $m \times m$ identity matrix is denoted \mathbf{I}_m . For a function $h : \mathbb{R} \rightarrow \mathbb{R}$ and a diagonal matrix $\mathbf{D} = \text{diag}(d_1, d_2, \dots, d_r)$, $h(\mathbf{D}) := \text{diag}(h(d_1), h(d_2), \dots, h(d_r))$.

2 Background on Grassmannian manifolds

Throughout this paper, we consider a Riemannian manifold on the space of subspaces called the Grassmannian manifold (Grassmann, 1862). Here we provide a brief background. For more details, we refer the readers to the seminal works by Edelman et al. (1998) and Absil et al. (2004); see also (Boumal, 2020, Ch. 9).

2.1 Riemannian geometry of Grassmannian manifolds

Grassmannian manifold. For $r \leq m$, the Grassmannian manifold $\text{Gr}(m, r)$ is the set of r -dimensional subspaces in \mathbb{R}^m . We consider the canonical Euclidean embedding into $\mathbb{R}^{m \times r}$, in which each point is represented by the equivalence class

$$[\mathbf{X}] = \{\mathbf{X}\mathbf{Q} : \mathbf{Q} \in \text{O}(r)\} \quad (2.1)$$

for $\mathbf{X} \in \mathbb{R}^{m \times r}$ such that $\mathbf{X}^\top \mathbf{X} = \mathbf{I}_r$. An equivalent way of representing $\text{Gr}(m, r)$ is via the quotient $\text{O}(m)/(\text{O}(r) \times \text{O}(m-r))$, where $\text{O}(d)$ is the orthogonal group of $d \times d$ matrices (Edelman et al., 1998).

Remark 1. From now on, we will often abuse notation and identify \mathbf{X} with the entire equivalence class $[\mathbf{X}]$ whenever it is clear from the context.

We now describe the Riemannian geometry of the Grassmann manifold. Since the Grassmannian manifold is a quotient manifold, for concreteness, it is convenient to work with a specific representative of the equivalent class. In the following, we choose and fix a representative element \mathbf{X} for a point $[\mathbf{X}] \in \text{Gr}(m, r)$.

Tangent space. First, the tangent space $\text{T}_{\mathbf{X}}\text{Gr}(m, r)$ at \mathbf{X} is given as

$$\text{T}_{\mathbf{X}}\text{Gr}(m, r) := \{ \Delta \in \mathbb{R}^{m \times r} : \mathbf{X}^\top \Delta = \mathbf{O} \} .$$

For any direction $\mathbf{D} \in \mathbb{R}^{m \times r}$, the projection of it onto the tangent space at \mathbf{X} is given as

$$(\mathbf{I}_m - \mathbf{X}\mathbf{X}^\top)\mathbf{D} \in \text{T}_{\mathbf{X}}\text{Gr}(m, r) .$$

Metric. The Riemannian metric on the Grassmann manifold is given as

$$\langle \Delta_1, \Delta_2 \rangle := \text{Tr}(\Delta_1^\top \Delta_2)$$

for $\Delta_1, \Delta_2 \in \text{T}_{\mathbf{X}}\text{Gr}(m, r)$.

Calculus. Now, we discuss Riemannian calculus on Grassmann manifolds. For a function $f : \text{Gr}(m, r) \rightarrow \mathbb{R}$, we define its gradient $\text{grad}f$ to be the vector field such that

$$\langle \text{grad}f(\mathbf{X}), \Delta \rangle = Df(\mathbf{X})[\Delta]$$

for any $\Delta \in \text{T}_{\mathbf{X}}\text{Gr}(m, r)$, where $Df(\mathbf{X})[\Delta]$ denotes the (Euclidean) directional derivative of f along the direction Δ . Moreover, the Hessian $\text{hess}f$ is the quadratic form (or the $(0, 2)$ -tensor) such that for any $\Delta \in \text{T}_{\mathbf{X}}\text{Gr}(m, r)$,

$$\text{hess}f(\mathbf{X})[\Delta, \Delta] = D(Df(\mathbf{X})[\Delta])[\Delta] .$$

2.2 Principal angles, distances and geodesics

Principal angles. In order to better understand Grassmannian geometry, we discuss a well-established notion from linear algebra called the *principal angles* between subspaces (Jordan, 1875). From (2.1), one can interpret each point \mathbf{X} on $\text{Gr}(m, r)$ as an equivalence class of orthonormal bases of $\text{col}(\mathbf{X})$. In other words, one can canonically identify each point on $\text{Gr}(m, r)$ with a r -dimensional subspace of \mathbb{R}^m . Now having this identification, we make the following definition about the principal angles.

Definition 1 (principal angles). For $[\mathbf{X}], [\mathbf{Y}]$ on $\text{Gr}(m, r)$, the principal angles between $[\mathbf{X}]$ and $[\mathbf{Y}]$ are defined as the principal angles between the subspaces $\text{col}(\mathbf{X})$ and $\text{col}(\mathbf{Y})$. In other words, denoting the singular values of $\mathbf{X}^\top \mathbf{Y}$ by $\lambda_1 \geq \dots \geq \lambda_r$, the principal angle matrix $\Theta \in \mathbb{R}^{r \times r}$ is the diagonal matrix whose (i, i) -th entry is $\arccos(\lambda_i) \in [0, \pi/2]$. We call each diagonal entry a principal angle.

The following proposition is an immediate consequence of the definition.

Proposition 1 (principal alignment). *For any given two points $[\mathbf{X}], [\mathbf{Y}]$ on $\text{Gr}(m, r)$, one can find two representatives $\mathbf{X}_p \in [\mathbf{X}]$ and $\mathbf{Y}_p \in [\mathbf{Y}]$ such that $\mathbf{X}_p^\top \mathbf{Y}_p = \cos(\Theta)$ where Θ is the principal angle matrix between $[\mathbf{X}]$ and $[\mathbf{Y}]$.*

Proof. Choose arbitrary representatives, say \mathbf{X} and \mathbf{Y} , of $[\mathbf{X}]$ and $[\mathbf{Y}]$, respectively. Let the singular value decomposition of $\mathbf{X}^\top \mathbf{Y}$ be $\mathbf{P}\Lambda\mathbf{Q}^\top$. Now choose $\mathbf{X}_p := \mathbf{X}\mathbf{P}$ and $\mathbf{Y}_p := \mathbf{Y}\mathbf{Q}$. Then, we have $\mathbf{X}_p^\top \mathbf{Y}_p = \mathbf{P}^\top \mathbf{X}^\top \mathbf{Y} \mathbf{Q} = \mathbf{P}^\top (\mathbf{P}\Lambda\mathbf{Q}^\top) \mathbf{Q} = \Lambda$, as desired. \square

Distances between subspaces. With the principal angles between subspaces, there are several well-established notions of distances; see (Edelman et al., 1998, §4.3). Here we write them as distances on $\text{Gr}(m, r)$.

Definition 2. For $[\mathbf{X}], [\mathbf{Y}] \in \text{Gr}(m, r)$, let Θ be the principal angle matrix between $[\mathbf{X}]$ and $[\mathbf{Y}]$. We define the following distances:

$$d_{\text{arc}}([\mathbf{X}], [\mathbf{Y}]) := \|\Theta\|_F \quad (\text{arc-length distance}), \quad (2.2)$$

$$d_{\text{chor}}([\mathbf{X}], [\mathbf{Y}]) := \|2 \sin(\Theta/2)\|_F \quad (\text{chordal distance}), \quad (2.3)$$

$$d_{\text{proj}}([\mathbf{X}], [\mathbf{Y}]) := \|\sin(\Theta)\|_F \quad (\text{projection distance}). \quad (2.4)$$

In fact, the arc-length distance is equal to the Riemannian distance (the distance determined by the Riemannian metric). Moreover, one can easily verify that the other two distances are equivalent metrics; see, e.g., (Keshavan et al., 2010, Remark 6.1).

Geodesics. It is known that when $m, r \geq 2$ there are at least countably many geodesics between two points on $\text{Gr}(m, r)$ (Wong, 1967). On the other hand, if all the principal angles between the two points are less than $\pi/2$, there is a unique geodesic of the shortest length (Wong, 1967).

Given two points $[\mathbf{X}], [\mathbf{Y}] \in \text{Gr}(m, r)$, let Θ be the principal angle matrix between $[\mathbf{X}]$ and $[\mathbf{Y}]$. Assume that all principal angles are less than $\pi/2$. Choosing representatives $\mathbf{X}_p \in [\mathbf{X}]$ and $\mathbf{Y}_p \in [\mathbf{Y}]$ as per Proposition 1, let $\Delta_p \in \mathbb{R}^{m \times r}$ be the orthonormal matrix such that

$$\mathbf{Y}_p = \mathbf{X}_p \cos(\Theta) + \Delta_p \sin(\Theta). \quad (2.5)$$

Such an orthonormal matrix Δ_p exists because $(\mathbf{I}_m - \mathbf{X}_p \mathbf{X}_p^\top) \mathbf{Y}_p$ belongs to the tangent space $\mathbb{T}_{\mathbf{X}_p} \text{Gr}(m, r)$. Then, with such choices of representatives, the geodesic $\mathbf{G}_p(t)$ of the shortest length joining the two points is given as

$$\mathbf{G}_p(t) = \mathbf{X}_p \cos(t\Theta) + \Delta_p \sin(t\Theta) \quad \text{for } t \in [0, 1]. \quad (2.6)$$

Note that this geodesic has the length $\|\Theta\|_F = d_{\text{arc}}([\mathbf{X}], [\mathbf{Y}])$.

We end our discussion by proving the following property that we will use later.

Lemma 2 (geodesic convexity). *For a fixed $[\mathbf{U}] \in \text{Gr}(m, r)$ and $\phi \in [0, \pi/4)$, let $\mathcal{N}_{[\mathbf{U}]}(\phi)$ be the subset of $\text{Gr}(m, r)$ consisting of points whose principal angles to $[\mathbf{U}]$ are all less than equal to ϕ , i.e., letting $\Theta_{[\mathbf{X}]}$ be the principal angle matrix between $[\mathbf{X}]$ and $[\mathbf{U}]$,*

$$\mathcal{N}_{[\mathbf{U}]}(\phi) := \{[\mathbf{X}] : \Theta_{[\mathbf{X}]} \preceq \phi \cdot \mathbf{I}\}.$$

Then, $\mathcal{N}_{[\mathbf{U}]}(\phi)$ is geodesically convex, i.e., for any two points $[\mathbf{X}], [\mathbf{Y}] \in \mathcal{N}_{[\mathbf{U}]}(\phi)$, the unique shortest geodesic joining them is entirely contained in $\mathcal{N}_{[\mathbf{U}]}(\phi)$.

Proof. We begin the proof by first invoking the variational characterization of the principal angles (see, e.g., (Miao and Ben-Israel, 1992)):

$$[\mathbf{X}] \in \mathcal{N}_{[\mathbf{U}]}(\phi) \iff \min_{\substack{\mathbf{x} \in \text{col}([\mathbf{X}]), \mathbf{u} \in \text{col}([\mathbf{U}]) \\ \|\mathbf{x}\|_2 = \|\mathbf{u}\|_2 = 1}} |\langle \mathbf{x}, \mathbf{u} \rangle| \geq \cos(\phi). \quad (2.7)$$

Now pick any two points $[\mathbf{X}]$ and $[\mathbf{Y}]$ from $\mathcal{N}_{[\mathbf{U}]}(\phi)$. Since $\phi < \pi/4$, it follows from (2.7) that the principal angles between $[\mathbf{X}]$ and $[\mathbf{Y}]$ are all less than equal to $2\phi < \pi/2$. Hence, there is a unique geodesic of the shortest length.

For concreteness, let us choose representatives as per (2.5). Also, let $\mathbf{G}_p(t)$ ($t \in [0, 1]$) be the unique geodesic of the shortest length between \mathbf{X}_p and \mathbf{Y}_p as in (2.6). For simplicity, we may assume that $\theta_i > 0$ for all $i \in [r]$. In fact, if $\theta_i = 0$, the i -th column of $\mathbf{G}_p(t)$ is constantly equal to the i -th column of \mathbf{X}_p along the geodesic. Hence, we have

$$\mathbf{G}_p(t) = \mathbf{X}_p \cos(t\Theta) + \Delta_p \sin(t\Theta) =: \mathbf{X}_p \mathbf{D}_1 + \mathbf{Y}_p \mathbf{D}_2,$$

where $\mathbf{D}_1 := (\cot(t\Theta) - \cot(\Theta)) \sin(t\Theta)$ and $\mathbf{D}_2 := [\sin(\Theta)]^{-1} \sin(t\Theta)$ are some diagonal matrices with nonnegative entries (since $\cot(\cdot)$ is decreasing on $[0, \pi/2]$).

Now in order to show that $[\mathbf{G}_p(t)] \in \mathcal{N}_{[\mathbf{U}]}(\phi)$, let us choose an arbitrary $\mathbf{g} \in \text{col}(\mathbf{G}_p(t))$. We can write $\mathbf{g} := \mathbf{G}_p(t)\boldsymbol{\lambda}$ for some $\boldsymbol{\lambda} \in \mathbb{R}^r$. Letting $\mathbf{x}_p := \mathbf{X}_p \mathbf{D}_1 \boldsymbol{\lambda}$ and $\mathbf{y}_p := \mathbf{Y}_p \mathbf{D}_2 \boldsymbol{\lambda}$,

$$\mathbf{g} = \mathbf{x}_p + \mathbf{y}_p \quad \text{and} \quad \langle \mathbf{x}_p, \mathbf{y}_p \rangle = \boldsymbol{\lambda}^\top \mathbf{D}_1^\top \cos(\Theta) \mathbf{D}_2 \boldsymbol{\lambda} \geq 0.$$

Based on this, we prove the following claim.

Claim. *Suppose that $\mathbf{x} \in \text{col}(\mathbf{X})$ and $\mathbf{y} \in \text{col}(\mathbf{Y})$ such that $\langle \mathbf{x}, \mathbf{y} \rangle \geq 0$, $\|\mathbf{x}\|_2 = \|\mathbf{y}\|_2 = 1$. Then, for any unit-norm vector $\mathbf{u} \in \text{col}(\mathbf{U})$, we have $\langle \mathbf{u}, \mathbf{x} \rangle \cdot \langle \mathbf{u}, \mathbf{y} \rangle > 0$.*

To prove this claim, suppose to the contrary that there exists a vector $\mathbf{u} \in \text{col}(\mathbf{U})$ such that $\langle \mathbf{u}, \mathbf{x} \rangle > 0$ but $\langle \mathbf{u}, \mathbf{y} \rangle < 0$. Then from (2.7), it follows that $\langle \mathbf{u}, \mathbf{x} \rangle > 1/\sqrt{2}$ and $\langle \mathbf{u}, \mathbf{y} \rangle < -1/\sqrt{2}$, since $\phi < \pi/4$. Then, using the hypothesis $\|\mathbf{x}\|_2 = \|\mathbf{y}\|_2 = 1$, this implies that

$$\sqrt{2} < \langle \mathbf{u}, \mathbf{x} - \mathbf{y} \rangle \leq \|\mathbf{u}\|_2 \|\mathbf{x} - \mathbf{y}\|_2 = \sqrt{2 - 2\langle \mathbf{x}, \mathbf{y} \rangle}.$$

Hence, it holds that $\langle \mathbf{x}, \mathbf{y} \rangle < 0$. This contradicts the hypothesis that $\langle \mathbf{x}, \mathbf{y} \rangle \geq 0$.

Now due to the claim, for any unit-norm $\mathbf{u} \in \text{col}(\mathbf{U})$, we have either (i) $\langle \mathbf{u}, \mathbf{x}_p / \|\mathbf{x}_p\|_2 \rangle \geq \cos(\phi)$ and $\langle \mathbf{u}, \mathbf{y}_p / \|\mathbf{y}_p\|_2 \rangle \geq \cos(\phi)$ or (ii) $\langle \mathbf{u}, \mathbf{x}_p / \|\mathbf{x}_p\|_2 \rangle \leq -\cos(\phi)$ and $\langle \mathbf{u}, \mathbf{y}_p / \|\mathbf{y}_p\|_2 \rangle \leq -\cos(\phi)$. Since \mathbf{g} is a unit-norm vector that is a conic combination of two vectors \mathbf{x}_p and \mathbf{y}_p , it follows that either (i) $\langle \mathbf{u}, \mathbf{g} \rangle \geq \cos(\phi)$ or (ii) $\langle \mathbf{u}, \mathbf{g} \rangle \leq -\cos(\phi)$. In other words, $|\langle \mathbf{u}, \mathbf{g} \rangle| \geq \cos(\phi)$ for any unit-norm $\mathbf{u} \in \text{col}(\mathbf{U})$. Since \mathbf{g} was arbitrarily chosen from $\text{col}(\mathbf{G}_p(t))$, this completes the proof. \square

Remark 2. When $\phi = \pi/4$, a careful inspection of the proof of Lemma 2 reveals that $\mathcal{N}_{[\mathbf{U}]}(\pi/4)$ is also geodesically convex in an appropriate sense: for any two point $[\mathbf{X}], [\mathbf{Y}] \in \mathcal{N}_{[\mathbf{U}]}(\phi)$, there is at least one geodesic of the shortest length joining them that is entirely contained in $\mathcal{N}_{[\mathbf{U}]}(\phi)$. However, one can see that this geodesic convexity is no longer true for $\phi > \pi/4$. For instance, for $\text{Gr}(2, 1)$, when $\phi = 3\pi/8$, choosing $[\mathbf{u}] = [(0, 1)^\top]$, $[\mathbf{x}] = [(\cos(\pi/8), \sin(\pi/8))^\top]$ and $[\mathbf{y}] = [(\cos(-\pi/8), \sin(-\pi/8))^\top]$, one can easily see that the unique geodesic between $[\mathbf{x}]$ and $[\mathbf{y}]$ is outside of $\mathcal{N}_{[\mathbf{u}]}(3\pi/8)$.

Remark 3. From the fact that Grassmann manifolds have sectional curvatures upper bounded by two (Wong, 1968), it follows from a classical result in Riemannian geometry (Klingenberg, 1959) that the convexity radius is greater than or equal to $\pi/4$. In light of this, Lemma 2 reveals that in fact for Grassmannian manifolds, the actual convexity radius is much larger than the classical lower bound.

3 Matrix factorization over a Grassmann manifold

In this section, we describe a formulation of the matrix factorization approach as an optimization over a Grassmannian manifold (Keshavan et al., 2010; Dai et al., 2011; Boumal and Absil, 2011; Dai et al., 2012; Boumal and Absil, 2015). First, consider the full observation case, i.e., $\Omega = [m] \times [n]$:

$$\underset{\substack{\mathbf{X} \in \mathbb{R}^{m \times r} \\ \mathbf{Y} \in \mathbb{R}^{n \times r}}}{\text{minimize}} \left[g_{\text{full}}(\mathbf{X}, \mathbf{Y}) := \frac{1}{2} \|\mathbf{X}\mathbf{Y}^\top - \mathbf{M}\|_{\text{F}}^2 \right]. \quad (3.1)$$

By symmetry, we have $g_{\text{full}}(\mathbf{X}, \mathbf{Y}) = g_{\text{full}}(\mathbf{X}^*\mathbf{R}, \mathbf{Y}^*(\mathbf{R}^{-1})^\top)$ for any invertible \mathbf{R} , and hence without loss generality, we may assume that \mathbf{X} is orthonormal. Now in order to reduce the number of optimization parameters, we optimize this cost function over \mathbf{Y} . Denoting $\mathbf{Y}_{\mathbf{X}} := \underset{\mathbf{Y} \in \mathbb{R}^{n \times r}}{\text{argmin}} g_{\text{full}}(\mathbf{X}, \mathbf{Y})$, the optimality condition yields:

$$0 = \nabla_2 g_{\text{full}}(\mathbf{X}, \mathbf{Y}_{\mathbf{X}}) = (\mathbf{X}\mathbf{Y}_{\mathbf{X}}^\top - \mathbf{M})^\top \mathbf{X}$$

which is equivalent to $\mathbf{Y}_{\mathbf{X}}\mathbf{X}^\top\mathbf{X} = \mathbf{M}^\top\mathbf{X}$. In particular, since \mathbf{X} is orthonormal, i.e., $\mathbf{X}^\top\mathbf{X} = \mathbf{I}_r$, we obtain $\mathbf{Y}_{\mathbf{X}} = \mathbf{M}^\top\mathbf{X}$. Plugging this back to (3.1), we arrive at the following optimization problem over $\text{Gr}(m, r)$:

$$\underset{\substack{\mathbf{X} \in \mathbb{R}^{m \times r} \\ \mathbf{Y} \in \mathbb{R}^{n \times r}}}{\text{minimize}} \left[f_{\text{full}}(\mathbf{X}) := \frac{1}{2} \|(\mathbf{I}_m - \mathbf{X}\mathbf{X}^\top)\mathbf{M}\|_{\text{F}}^2 \right]. \quad (3.2)$$

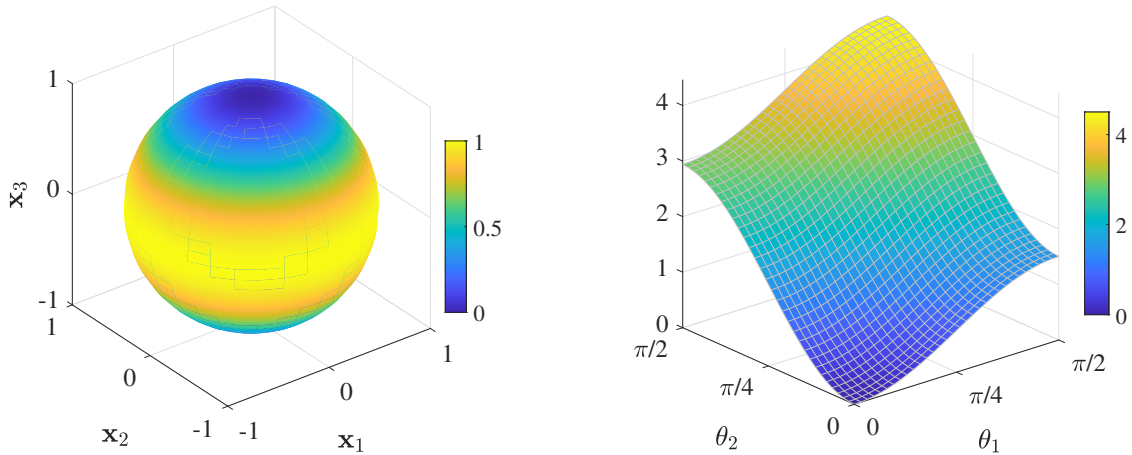


Figure 1: Illustration of the fully observed cost (3.2). (Left) The rank-one case with $\sigma = \sqrt{2}$ and $\mathbf{u} = (0, 0, 1)$. (Right) Illustration of the landscape for the rank-6 case using two principal angles to the ground truth $[\mathbf{U}]$. We set $m = 100$, $n = 200$, and $\Sigma = \text{diag}(1, 1, 1, 1.4, 1.4, 1.4)$.

Note that $f_{\text{full}}(\mathbf{X}\mathbf{Q}) = f_{\text{full}}(\mathbf{X})$ for any $\mathbf{Q} \in \mathcal{O}(r)$ and hence (3.2) is well-defined on $\text{Gr}(m, r)$. The above derivation can be also found in (Pitaval et al., 2015, §III-A).

Remark 4. A similar objective function was considered in (Maunu et al., 2019) under the context of robust subspace recovery.

To have a glimpse of the cost (3.2), we illustrate it for the simplest case of rank-1 and full observation. Assume that $\mathbf{M} = \sigma \mathbf{u}\mathbf{v}^\top$ for unit vectors \mathbf{u} and \mathbf{v} and $\sigma > 0$. Using \mathbf{x} to denote the argument of the cost function, (3.2) becomes

$$f_{\text{full}}(\mathbf{x}) = \frac{1}{2} \|(\mathbf{I}_m - \mathbf{x}\mathbf{x}^\top)\mathbf{M}\|_{\text{F}}^2 = \frac{\sigma^2}{2} \|(\mathbf{I}_m - \mathbf{x}\mathbf{x}^\top)\mathbf{u}\mathbf{v}^\top\|_{\text{F}}^2.$$

See Figure 1 for the landscape for this simplest case.

In general, when only partially observed entries are available, we have

$$\underset{\substack{\mathbf{X} \in \mathbb{R}^{m \times r} \\ \mathbf{Y} \in \mathbb{R}^{n \times r}}}{\text{minimize}} \left[g(\mathbf{X}, \mathbf{Y}) := \frac{1}{2} \|\mathbf{X}\mathbf{Y}^\top - \mathbf{M}\|_{\Omega}^2 \right].$$

Similarly to the fully observed case, one can reduce the number of parameters by considering $\mathbf{Y}_{\mathbf{X}} := \text{argmin}_{\mathbf{Y} \in \mathbb{R}^{n \times r}} g(\mathbf{X}, \mathbf{Y})$. Then, we obtain the optimization problem

$$\underset{\mathbf{X} \in \mathbb{R}^{m \times r}, \mathbf{X}^\top \mathbf{X} = \mathbf{I}}{\text{minimize}} \left[f(\mathbf{X}) := \min_{\mathbf{Y} \in \mathbb{R}^{n \times r}} g(\mathbf{X}, \mathbf{Y}) \right].$$

In the subsequent section, we first focus on understanding the fully observed case. We will continue our discussion regarding the partially observed case in Section 5.

3.1 Interpretation based on the projection distance

To better understand the formulation, we provide a fruitful interpretation for the full observation cost (3.2). Our interpretation will be based on the principal angle and the distances introduced in Section 2.2. For setup, we make the following choice of representative elements in the equivalence class, motivated by Proposition 1. We call this choice the *principal alignment*, and we will repeatedly use this choice in later calculations:

Principal alignment. Let Θ be the principal angle matrix between $[\mathbf{X}]$ and $[\mathbf{U}]$.

1. By Proposition 1, there exist $\mathbf{X}_p \in [\mathbf{X}]$, $\mathbf{U}_p \in [\mathbf{U}]$ s.t. $\mathbf{X}_p^\top \mathbf{U}_p = \cos(\Theta)$.

2. Let $\Delta_p \in \mathbb{T}_{\mathbf{X}_p} \text{Gr}(m, r)$ be an orthonormal matrix s.t. $\Delta_p \sin(\Theta) = (\mathbf{I}_m - \mathbf{X}_p \mathbf{X}_p^\top)^\top \mathbf{U}_p$.

Write $\mathbf{U}_p = \mathbf{U}\mathbf{Q}$ for $\mathbf{Q} \in \mathcal{O}(r)$. Let $\Xi := \mathbf{Q}^\top \Sigma^2 \mathbf{Q} \in \mathbb{R}^{r \times r}$ and $\xi_i := \Xi_{i,i}$ for $i \in [r]$. Note that $\sigma_{\min}^2 \leq \xi_i \leq \sigma_{\max}^2$ for all $i \in [r]$.

Remark 5. $\Theta, \Delta_p, \mathbf{Q}, \Xi$ all depend on the point $[\mathbf{X}]$.

With the **principal alignment**, it is easy to see that

$$\begin{aligned} f_{\text{full}}(\mathbf{X}) &= \frac{1}{2} \|(\mathbf{I}_m - \mathbf{X}_p \mathbf{X}_p^\top) \mathbf{U}_p \mathbf{Q}^\top \Sigma \mathbf{V}^\top\|_{\text{F}}^2 \\ &= \frac{1}{2} \|\Delta_p \sin(\Theta) \mathbf{Q}^\top \Sigma\|_{\text{F}}^2 = \frac{1}{2} \text{Tr}[\sin^2(\Theta) \Xi]. \end{aligned}$$

See Figure 1 for an illustration of the landscape based on the principal angles to $[\mathbf{U}]$. Therefore, we arrive at the following interpretation:

The cost f_{full} is equal to a weighted projection distance.

Having this interpretation, we now study the geometry of the cost function.

4 Geometry of the fully observed case

In this section, we study the geometry of the full observation cost f_{full} defined in (3.2). Let us first compute the derivatives. For any $\Delta \in \mathbb{T}_{\mathbf{X}} \text{Gr}(m, r)$,

$$\begin{aligned} \langle \text{grad} f_{\text{full}}(\mathbf{X}), \Delta \rangle &= Df_{\text{full}}(\mathbf{X})[\Delta] \\ &= -\frac{1}{p} \langle (\Delta \mathbf{X}^\top + \mathbf{X} \Delta^\top) \mathbf{M}, (\mathbf{I}_m - \mathbf{X} \mathbf{X}^\top) \mathbf{M} \rangle_{\Omega}. \end{aligned} \quad (4.1)$$

$$\begin{aligned} \text{hess} f_{\text{full}}(\mathbf{X})[\Delta, \Delta] &= D(\text{grad} f_{\text{full}}(\mathbf{X})[\Delta])[\Delta] \\ &= -\frac{2}{p} \langle \Delta \Delta^\top \mathbf{M}, (\mathbf{I}_m - \mathbf{X} \mathbf{X}^\top) \mathbf{M} \rangle_{\Omega} + \frac{1}{p} \|(\Delta \mathbf{X}^\top + \mathbf{X} \Delta^\top) \mathbf{M}\|_{\Omega}^2. \end{aligned} \quad (4.2)$$

4.1 Geometry based on gradient

We first derive a compact expression for gradient based on the principal angles.

Theorem 1 (characterization of gradient). *Assume $\Omega = [m] \times [n]$. Let $[\mathbf{X}] \in \text{Gr}(m, r)$. With the **principal alignment**, the gradient has the following compact expression:*

$$\text{grad} f_{\text{full}}(\mathbf{X}_p) = -\Delta_p \sin(\Theta) \Xi \cos(\Theta). \quad (4.3)$$

Consequently, $\frac{\sigma_{\min}^4}{4} \|\sin(2\Theta)\|_{\text{F}}^2 \leq \|\text{grad} f_{\text{full}}([\mathbf{X}])\|_{\text{F}}^2 \leq \frac{\sigma_{\max}^4}{4} \|\sin(2\Theta)\|_{\text{F}}^2$.

Proof. Rewriting the first derivative (4.1) under the **principal alignment**, $\langle \text{grad} f_{\text{full}}(\mathbf{X}_p), \Delta \rangle$ can be written as

$$-\langle (\Delta \mathbf{X}_p^{\top} + \mathbf{X}_p \Delta^{\top}) \mathbf{M}, (\mathbf{I}_m - \mathbf{X}_p \mathbf{X}_p^{\top}) \mathbf{M} \rangle.$$

On the other hand, using the fact that $(\mathbf{I}_m - \mathbf{X}_p \mathbf{X}_p^{\top}) \mathbf{X}_p = \mathbf{O}$, the second term in the above expression vanishes: $\langle \mathbf{X}_p \Delta^{\top} \mathbf{M}, (\mathbf{I}_m - \mathbf{X}_p \mathbf{X}_p^{\top}) \mathbf{M} \rangle = \langle (\mathbf{I}_m - \mathbf{X}_p \mathbf{X}_p^{\top}) \mathbf{X}_p \Delta^{\top} \mathbf{M}, \mathbf{M} \rangle = 0$. Thus, after rearranging, we obtain the desired compact expression:

$$\begin{aligned} \text{grad} f_{\text{full}}(\mathbf{X}_p) &= -(\mathbf{I}_m - \mathbf{X}_p \mathbf{X}_p^{\top}) \mathbf{M} \mathbf{M}^{\top} \mathbf{X}_p \\ &= -(\mathbf{I}_m - \mathbf{X}_p \mathbf{X}_p^{\top}) \mathbf{U}_p \mathbf{Q}^{\top} \Sigma^2 \mathbf{Q} \mathbf{U}_p^{\top} \mathbf{X}_p \\ &= -\Delta_p \sin(\Theta) \Xi \cos(\Theta). \end{aligned}$$

Now, the last part of the theorem follows due to the definition of Ξ together with the basic trigonometric fact $\sin(2\theta) = 2 \sin(\theta) \cos(\theta)$. \square

We remark that a similar calculation is done in (Pitaval et al., 2015, §III). With Theorem 1, the following characterization of critical points is immediate.

Corollary 2 (critical points). *Assume $\Omega = [m] \times [n]$. Let $[\mathbf{X}]$ be a point on $\text{Gr}(m, r)$, and $\theta_1, \dots, \theta_r$ be the principal angles between $[\mathbf{X}]$ and $[\mathbf{U}]$. Then, $[\mathbf{X}]$ is a critical point of f_{full} if and only if $\theta_i = 0$ or $\pi/2 \forall i \in [r]$.*

4.2 Geometry based on Hessian

We first derive a compact expression for Hessian based on the principal angles.

Theorem 3 (characterization of the Hessian). *Assume $\Omega = [m] \times [n]$. Let $[\mathbf{X}] \in \text{Gr}(m, r)$. With the **principal alignment**, the second derivative $\text{hess} f_{\text{full}}(\mathbf{X}_p)[\Delta, \Delta]$ has the following compact expression: for any direction $\Delta \in \mathbb{T}_{\mathbf{X}_p} \text{Gr}(m, r)$,*

$$\text{Tr} [\cos(\Theta) \Delta^{\top} \Delta \cos(\Theta) \Xi] - \text{Tr} [\sin(\Theta) \Delta_p^{\top} \Delta \Delta^{\top} \Delta_p \sin(\Theta) \Xi]. \quad (4.4)$$

Proof. Rewriting the second derivative (4.2) under the **principal alignment**,

$$-2 \langle \Delta \Delta^\top \mathbf{M}, (\mathbf{I}_m - \mathbf{X}_p \mathbf{X}_p^\top) \mathbf{M} \rangle + \|(\Delta \mathbf{X}_p^\top + \mathbf{X}_p \Delta^\top) \mathbf{M}\|_F^2.$$

We will simplify the above two terms one by one.

First, from the **principal alignment**, note that $(\mathbf{I}_m - \mathbf{X}_p \mathbf{X}_p^\top) \mathbf{M} = \Delta_p \sin(\Theta) \mathbf{Q}^\top \Sigma \mathbf{V}^\top$. Hence, using the fact that $(\mathbf{I}_m - \mathbf{X}_p \mathbf{X}_p^\top) \Delta = \Delta$, we have

$$\begin{aligned} \langle \Delta \Delta^\top \mathbf{M}, (\mathbf{I}_m - \mathbf{X}_p \mathbf{X}_p^\top) \mathbf{M} \rangle &= \langle \Delta \Delta^\top, (\mathbf{I}_m - \mathbf{X}_p \mathbf{X}_p^\top) \mathbf{M} \mathbf{M}^\top (\mathbf{I}_m - \mathbf{X}_p \mathbf{X}_p^\top) \rangle \\ &= \langle \Delta \Delta^\top, \Delta_p \sin(\Theta) \Xi \sin(\Theta) \Delta_p^\top \rangle \\ &= \text{Tr} \left[\left(\sin(\Theta) \Delta_p^\top \Delta \Delta^\top \Delta_p \sin(\Theta) \Xi \right) \right]. \end{aligned} \quad (4.5)$$

Hence, it follows that the first term is equal to $-2 \text{Tr} \left[\left(\sin(\Theta) \Delta_p^\top \Delta \Delta^\top \Delta_p \sin(\Theta) \Xi \right) \right]$.

Next we calculate the second term. First, expanding out the Frobenius norm, we obtain

$$\|\Delta \mathbf{X}_p^\top \mathbf{M}\|_F^2 + 2 \langle \Delta \mathbf{X}_p^\top \mathbf{M}, \mathbf{X}_p \Delta^\top \mathbf{M} \rangle + \|\mathbf{X}_p \Delta^\top \mathbf{M}\|_F^2.$$

Note that the middle term is 0 since $(\mathbf{I}_m - \mathbf{X}_p \mathbf{X}_p^\top) \mathbf{X}_p = \mathbf{O}$. Moreover, one can easily check that the third term is equal to (4.5):

$$\|\mathbf{X}_p \Delta^\top \mathbf{M}\|_F^2 = \|\Delta^\top \mathbf{M}\|_F^2 = \langle \Delta \Delta^\top \mathbf{M}, \mathbf{M} \mathbf{M}^\top \rangle = (4.5).$$

Therefore, the three terms above is equal to

$$\|\Delta \mathbf{X}_p^\top \mathbf{M}\|_F^2 + \text{Tr} \left[\left(\sin(\Theta) \Delta_p^\top \Delta \Delta^\top \Delta_p \sin(\Theta) \Xi \right) \right].$$

Now, let us calculate $\|\Delta \mathbf{X}_p^\top \mathbf{M}\|_F^2$. Using the definition of Ξ , we have $\langle \Delta \mathbf{X}_p^\top \mathbf{M}, \Delta \mathbf{X}_p^\top \mathbf{M} \rangle = \langle \mathbf{X}_p \Delta^\top \Delta \mathbf{X}_p^\top, \mathbf{M} \mathbf{M}^\top \rangle = \langle \mathbf{X}_p \Delta^\top \Delta \mathbf{X}_p^\top, \mathbf{U}_p \Xi \mathbf{U}_p^\top \rangle = \text{Tr} [\cos(\Theta) \Delta^\top \Delta \cos(\Theta) \Xi]$.

Combining the above calculations, we obtain the desired expression. \square

With the compact expression for Hessian, one can characterize the landscape of the cost function. See Figure 2 for illustrations of the landscape.

Corollary 4 (landscape based on Hessian). *Assume $\Omega = [m] \times [n]$. Let $[\mathbf{X}] \in \text{Gr}(m, r)$, and $\theta_1, \dots, \theta_r$ be the principal angles between $[\mathbf{X}]$ and $[\mathbf{U}]$.*

1. *If $\theta_i \in [0, \pi/4] \forall i \in [r]$, then $\text{hess}f_{\text{full}}([\mathbf{X}])[\Delta, \Delta]$ is nonnegative for any $\Delta \in \mathbb{T}_{[\mathbf{X}]} \text{Gr}(m, r)$.*
2. *If $\theta_i > \pi/4$ for some $i \in [r]$, then there exists a direction $\Delta \in \mathbb{T}_{[\mathbf{X}]} \text{Gr}(m, r)$ along which the second derivative is negative.*

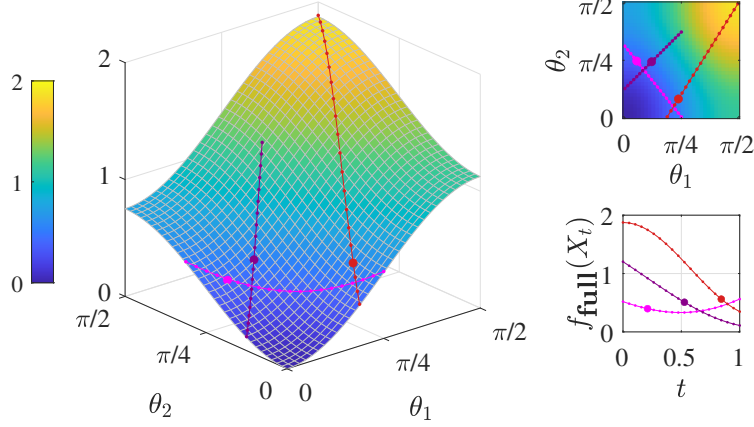


Figure 2: Illustrations of the landscape of cost function f_{full} . We choose the same parameters as in Figure 1. We overlay three geodesics with bigger dots that represent the points where the geodesics enter the region $\mathcal{N}_{[\cup]}(\pi/4)$.

Proof. To parse the expression for the second derivative (4.4), we rewrite the direction $\Delta \in \mathbb{T}_{\mathbf{X}_p} \text{Gr}(m, r)$, as $\bar{\Delta} \sin \Phi$, where $\bar{\Delta}$ is orthonormal, i.e., $\bar{\Delta}^\top \bar{\Delta} = \mathbf{I}_r$ and $\Phi = \text{diag}(\phi_1, \dots, \phi_r) \in \mathbb{R}^{r \times r}$ is a diagonal matrix with entries in $[0, \pi/2]$. Then, the second derivative (4.4) becomes

$$\text{Tr} [\sin^2(\Phi) \cos^2(\Theta) \Xi] - \text{Tr} [\sin(\Theta) \Delta_p^\top \bar{\Delta} \sin^2(\Phi) \bar{\Delta}^\top \Delta_p \sin(\Theta) \Xi]. \quad (4.6)$$

Having this expression, we consider the two cases in the statement separately:

1. First suppose that $\theta_i \in [0, \pi/4] \forall i \in [r]$. Then, we have $\sin(\theta_i) \leq 1/\sqrt{2} \leq \cos(\theta_i) \forall i \in [r]$. From this, one can see that

$$\sin(\Theta) \Delta_p^\top \bar{\Delta} \sin^2(\Phi) \bar{\Delta}^\top \Delta_p \sin(\Theta) \preceq 1/2 \sin^2(\Phi).$$

On the other hand, since Ξ is a PSD matrix,

$$(4.6) \geq \text{Tr}[\sin^2(\Phi) (\cos^2(\Theta) - 1/2 \mathbf{I}_r) \Xi] \geq 0.$$

2. Next, suppose that $\theta_i > \pi/4$ for some $i \in [r]$. Then, $\cos^2(\theta_i) - \sin^2(\theta_i) < 0$. Now, choose $\bar{\Delta} = \Delta_p$ and Φ so that $\phi_i = \pi/2$ and $\phi_j = 0$ for all $j \neq i$. With such a choice, (4.6) becomes $\xi_i(\cos^2(\theta_i) - \sin^2(\theta_i)) < 0$.

This completes the proof of Corollary 4. □

In fact, the proof reveals that if $\theta_1, \dots, \theta_r \in [0, \phi]$ for some $\phi < \pi/4$, the second derivative is greater than equal to $\min_{i \in [r]} [\xi_i \cdot (\cos^2(\phi) - \sin^2(\phi))]$. This together with the geodesic convexity of $\mathcal{N}_{[\cup]}(\phi)$ (Lemma 2) shows that the cost f_{full} is strongly geodesically-convex.

Corollary 5 (geodesic convexity). Assume $\Omega = [m] \times [n]$ and $\phi \in [0, \pi/4)$. Following the notations from Lemma 2, for any $[\mathbf{X}], [\mathbf{Y}] \in \mathcal{N}_{[\mathbf{U}]}(\phi)$, we have

$$f_{\text{full}}(\mathbf{Y}) \geq f_{\text{full}}(\mathbf{X}) + \langle \text{grad} f_{\text{full}}(\mathbf{X}), (\mathbf{I}_m - \mathbf{X}\mathbf{X}^\top)\mathbf{Y} \rangle + \frac{\mu}{2} d_{\text{arc}}(\mathbf{X}, \mathbf{Y})^2,$$

where $\mu := \sigma_{\min} \cdot (\cos^2(\phi) - \sin^2(\phi))$. In other words, f_{full} is μ -strongly geodesically-convex in $\mathcal{N}_{[\mathbf{U}]}(\phi)$. Moreover, f_{full} is geodesically-convex in $\mathcal{N}_{[\mathbf{U}]}(\pi/4)$.

Next, Corollaries 2 and 4 together conclude that all critical points are strict saddle points. In other words, there is no spurious local minima for f_{full} . We formally write this conclusion below. Note that this conclusion is consistent with the previously results in the Euclidean domain (Ge et al., 2016, 2017).

Corollary 6 (escaping direction). Assume $\Omega = [m] \times [n]$. Suppose that $[\mathbf{X}] \in \text{Gr}(m, r)$ is a critical point of f_{full} , and let $\Theta = \text{diag}(\theta_1, \dots, \theta_r)$ be the principal angle matrix between $[\mathbf{X}]$ and $[\mathbf{U}]$. Then the following hold:

- (Corollary 2) Each θ_i is equal to either 0 or $\pi/2$.
- (Corollary 4) With the **principal alignment**, the direction $\Delta_{\text{crit}} \in \mathbb{T}_{\mathbf{X}_p} \text{Gr}(m, r)$ defined as $\mathbf{U}_p \sin(\Theta)$ (i.e., the i -th column of Δ_{crit} equals that of \mathbf{U}_p if $\theta_i = \pi/2$ and $\mathbf{0}$ if $\theta_i = 0$) satisfies $\text{hess} f_{\text{full}}(\mathbf{X}_p)[\Delta_{\text{crit}}, \Delta_{\text{crit}}] = -\text{Tr}(\sin^2(\Theta)\Xi) < 0$.

Proof. The first statement is the restatement of Corollary 2. For the second statement, first note from (4.6) that $\text{hess} f_{\text{full}}([\mathbf{X}])[\Delta_p \sin(\Theta), \Delta_p \sin(\Theta)]$ is equal to

$$\text{Tr} \left[\left(\sin^2(\Theta)(\cos^2(\Theta) - \sin^2(\Theta)) \right) \Xi \right] = -\text{Tr} [\sin^2(\Theta)\Xi],$$

where the equality follows from the fact that each θ_i is equal to either 0 or $\pi/2$. From the **principal alignment**, $\Delta_p \sin(\Theta) = (\mathbf{I}_m - \mathbf{X}_p \mathbf{X}_p^\top)^\top \mathbf{U}_p = \mathbf{U}_p \sin(\Theta)$, where again the equality holds since each θ_i is equal to either 0 or $\pi/2$. Hence, in fact $\Delta_p \sin(\Theta) = \Delta_{\text{crit}}$. \square

5 Geometry of the partially observed case

In this section, we empirically study the geometry of the partially observed case based on our findings in Section 4. For simplicity, we focus on a simple *uniform* observation model where each entry of \mathbf{M} is observed independently with probability $p \in (0, 1]$.

We recall the formulation for the partially observed case.

$$\begin{aligned} & \underset{\mathbf{X} \in \mathbb{R}^{m \times r}, \mathbf{X}^\top \mathbf{X} = \mathbf{I}}{\text{minimize}} \left[f(\mathbf{X}) := \frac{1}{p} \cdot \min_{\mathbf{Y} \in \mathbb{R}^{n \times r}} g(\mathbf{X}, \mathbf{Y}) \right], \\ & \text{where } g(\mathbf{X}, \mathbf{Y}) := \frac{1}{2} \|\mathbf{X}\mathbf{Y}^\top - \mathbf{M}\|_\Omega^2. \end{aligned} \tag{5.1}$$

In fact, we multiply the cost by $1/p$ for a correct scale. We first empirically study the landscape of this formulation. Later in this section, we discuss some variants of this formulation considered in previous works.

5.1 Landscape simulations

Settings. We follow the setups considered in (Boumal and Absil, 2015, §5). For all setups, orthonormal matrices $\mathbf{U} \in \mathbb{R}^{m \times r}$ and $\mathbf{V} \in \mathbb{R}^{n \times r}$ are generated uniformly at random.

- *Setting 1: rectangular matrices.* We set $m = 1000$, $n = 30\,000$, $r = 6$ and $\Sigma = \text{diag}(1, 1 + \frac{1}{5}, \dots, 1 + \frac{4}{5}, 2)$.
- *Setting 2: high dimension.* We set $m = n = 10\,000$, $r = 10$ and $\Sigma = \text{diag}(1, 1 + \frac{1}{9}, \dots, 1 + \frac{8}{9}, 2)$.
- *Setting 3: bad conditioning.* We set $m = n = 1000$, $r = 10$. To make the ground truth matrix ill-conditioned, we set $\Sigma = \sqrt{mn} \cdot \text{diag}(1, e^{5/9}, e^{10/9}, \dots, e^{40/9}, e^5)$.

Simulations. Under the above scenarios, we run the following experiments. See Figures 3, 4 and 5 for the results.

1. *Landscapes for the settings in (Boumal and Absil, 2015).* We first illustrate the landscape of f for the choice of sampling probabilities in (Boumal and Absil, 2015, §5): $p = 0.026$ for Setting 1, $p = 0.006$ for Setting 2, and $p = 0.01$ for Setting 3. We compare them with the $p = 1$ case. As one can see from the top-left plot of Figures 3, 4 and 5, the landscapes are very similar to the fully observed case.
2. *Evolution of cost for varying p .* We next plot the evolution of the expected cost value $\mathbb{E} f(\mathbf{X})$ as we vary the sampling probability p . For each setting, we generate six points $\{\mathbf{X}_1, \dots, \mathbf{X}_6\}$ randomly from $\text{Gr}(m, r)$ whose principal angles to the ground truth matrix all lie between $\frac{\pi}{4}$ and $\frac{3\pi}{4}$. Then for each point \mathbf{X}_i , we compute $\mathbb{E} f(\mathbf{X}_i)$ as we vary the sampling probability p . To compute the expected cost value, we run 100 independent trials and compute the average. We also depict the error bars with shades. As one can see from the top-right plot of Figures 3, 4 and 5, the cost values decrease while keeping the relative ratio similar as p decreases. Also, notice that the cost values are well concentrated around their averages (the error bar shades are only noticeable for Setting 3).
3. *Comparison of landscape for varying p .* For each setting, we compare the landscape of f for sampling probabilities $p = 1, 0.1, 0.01, 0.001$. As one can see from the bottom plot of Figures 3, 4 and 5, the landscapes for $p = 0.1, 0.01$ are almost identical to those for $p = 1$. Experiment 3 demonstrates that the landscapes of the partially observed case are greatly similar to those of the fully observed case unless p is too small.

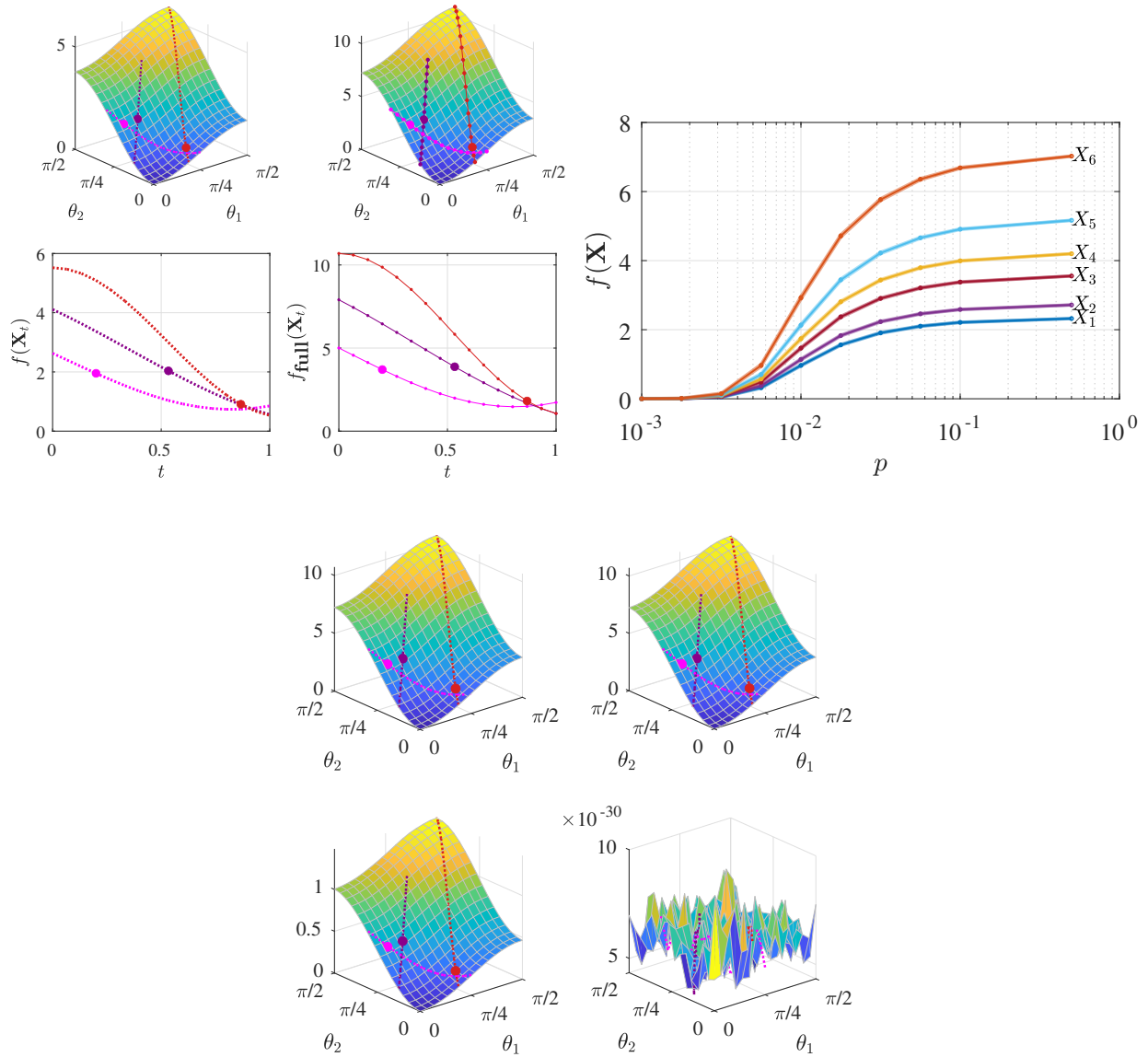


Figure 3: Simulation results for Setting 1. (Top-left) Results for Experiment 1. Note that the landscape ($p = 0.026$) is very similar to the fully observed case ($p = 1$). (Top-right) Results for Experiment 2. We depict the error bars with shades around each curve. (Bottom) Results for Experiment 3. Note that for $p = 0.1, 0.01$ the landscapes are quite similar to the fully observed case ($p = 1$).

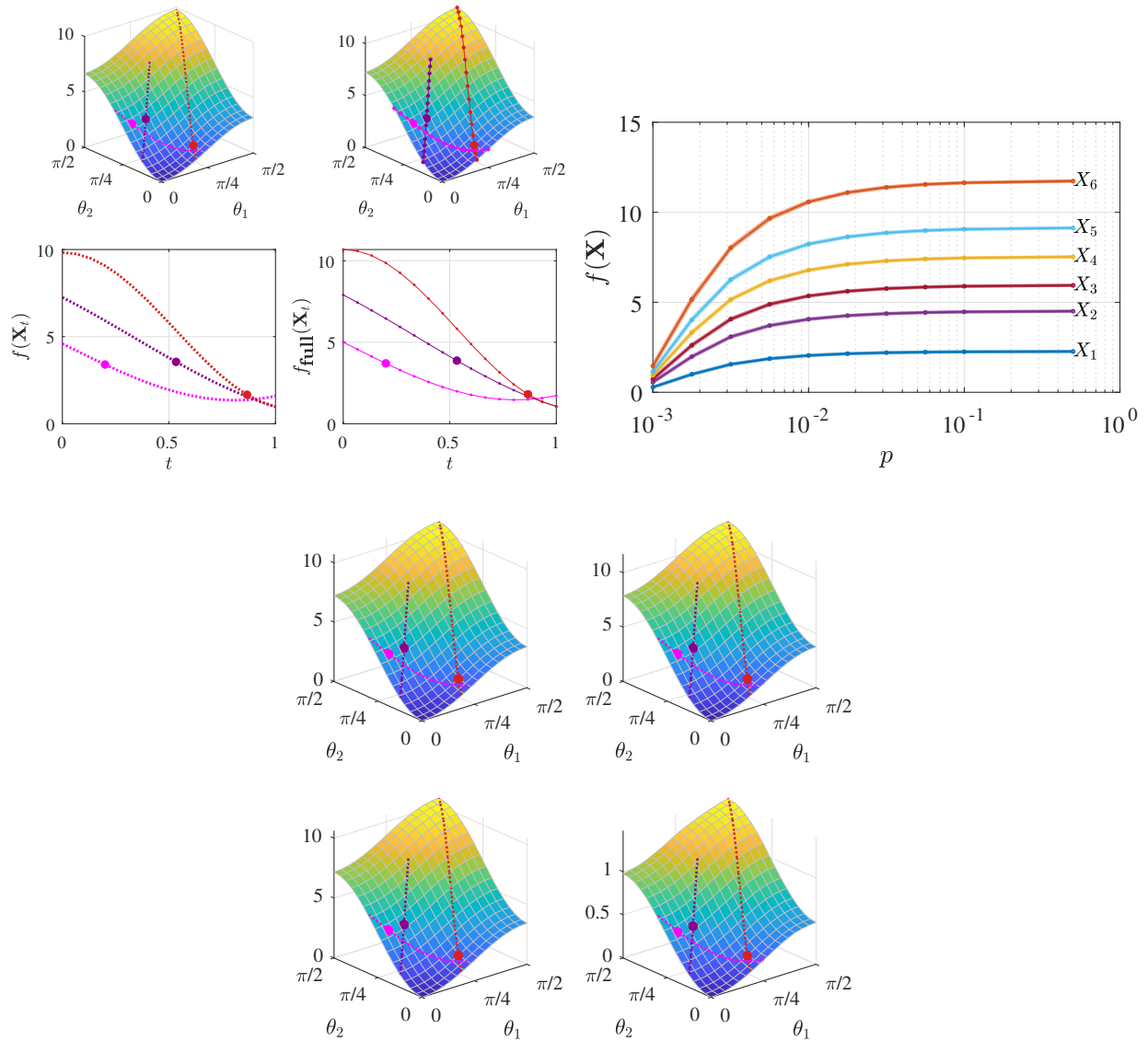


Figure 4: Simulation results for Setting 2. (Top-left) Results for Experiment 1. Note that the landscape ($p = 0.006$) is very similar to the fully observed case ($p = 1$). (Top-right) Results for Experiment 2. We depict the error bars with shades around each curve. (Bottom) Results for Experiment 3. Note that the landscapes are quite similar to the fully observed case ($p = 1$).

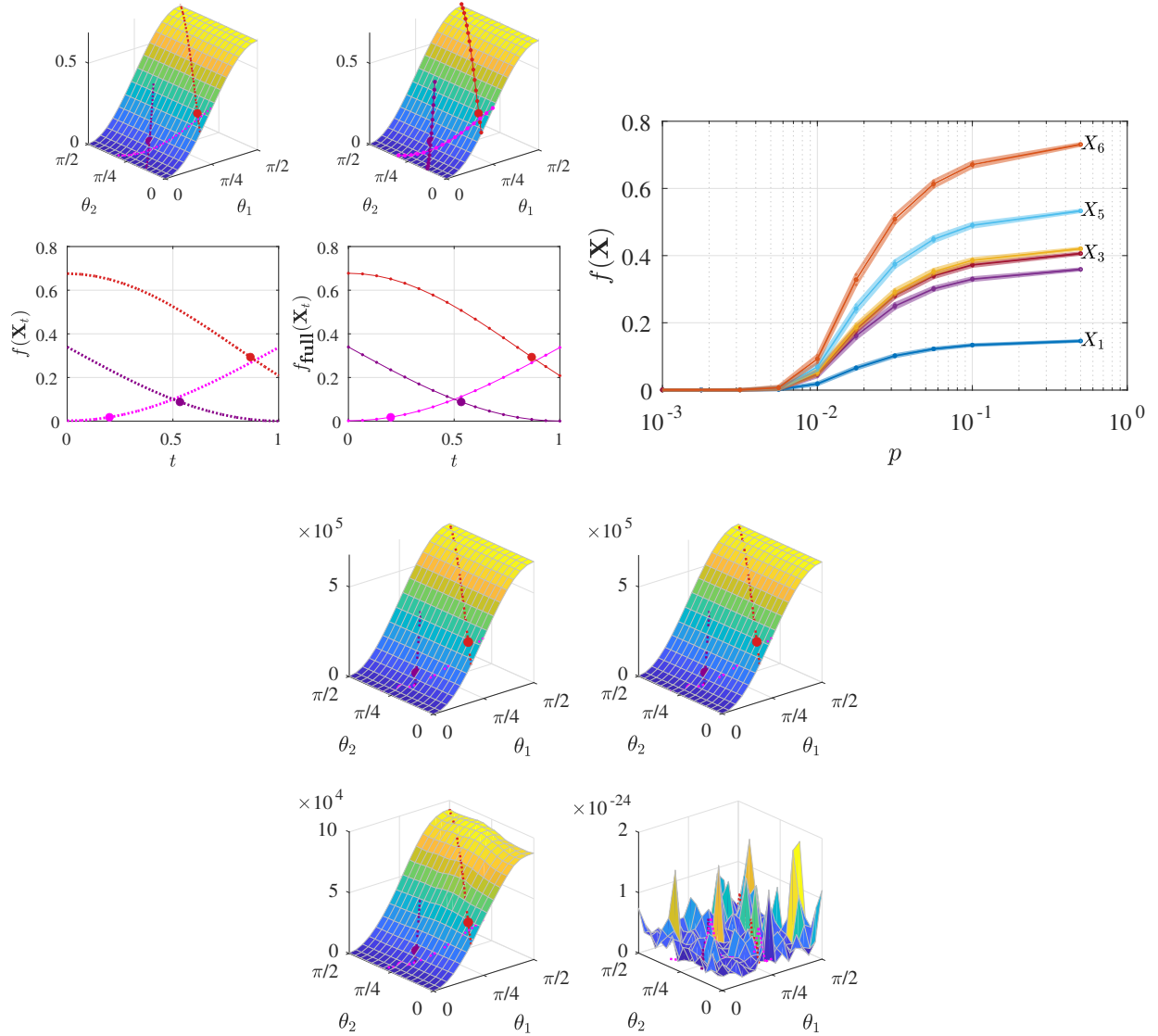


Figure 5: Simulation results for Setting 3. (Top-left) Results for Experiment 1. Note that the landscape ($p = 0.1$) is very similar to the fully observed case ($p = 1$). (Top-right) Results for Experiment 2. We depict the error bars with shades around each curve. (Bottom) Results for Experiment 3. Note that for $p = 0.1, 0.01$ the landscapes are quite similar to the fully observed case ($p = 1$).

5.2 Other formulations

In this section, we discuss other formulations considered in previous works (Dai et al., 2012; Boumal and Absil, 2015). First, we note that the cost function (5.1) could become discontinuous in general. To formally see this, let us revisit (Dai et al., 2012, Example 1).

Example 1. Consider a toy example where the ground truth matrix \mathbf{M} is equal to $[0, 1, 1]^\top$ and $\Omega = \{2, 3\}$, i.e., the two entries of value 1 are observed. Now let us consider the cost at the point $\mathbf{x} = [\sqrt{1 - 2\epsilon^2}, \epsilon, \epsilon]^\top$ for $\epsilon \in [0, 1/\sqrt{2}]$. From (5.1),

$$\begin{aligned} f(\mathbf{u}) &= \frac{3}{4} \cdot \min_{y \in \mathbb{R}} \|y\mathbf{x} - [0, 1, 1]^\top\|_\Omega^2 = \frac{3}{2} \cdot \min_{y \in \mathbb{R}} (1 - \epsilon y)^2 \\ &= \begin{cases} 0 & \text{if } \epsilon \in (0, 1/\sqrt{2}], \\ 3/2 & \text{if } \epsilon = 0. \end{cases} \end{aligned}$$

Hence, one can see that f for this toy example is discontinuous at $\mathbf{x} = [1, 0, 0]^\top$.

To remedy this discontinuity issue, (Dai et al., 2012) consider a different formulation based on the chordal distance, and (Boumal and Absil, 2015) add a regularization term to the cost function. These modifications are indeed shown to be useful for real applications (see (Boumal and Absil, 2015, §6) or (Keshavan and Oh, 2009, §3.4)).

6 Discussion

We conclude this paper with several relevant open questions.

Extension to the partially observed case. We have seen in Section 5 that the landscapes for the partially observed case are greatly similar to those for the fully observed case unless p is too small. Hence, one future direction is to extend our theoretical results in Section 4 to the partially observed case.

Optimization aspect. Our main results characterize the Grassmannian landscape of (3.2). It is then natural to ask the optimization aspect of our findings. Since our landscape analysis reveals the (strong) geodesic convexity of the cost within the basin $\mathcal{N}_{[\mathbf{U}]}(\pi/4)$, gradient methods converges fast within the basin. It would be then interesting to see how the gradient methods (or other optimization methods) behave outside the basin. Our preliminary experiment on the trajectories of Riemannian gradient descent is reported in Figure 6. Also, investigating other conditions for fast optimization (e.g., Polyak-Łojasiewicz (PL) inequality) would be an interesting direction. Lastly, whether one could develop a new optimization method based on our results is also an intriguing direction to pursue.

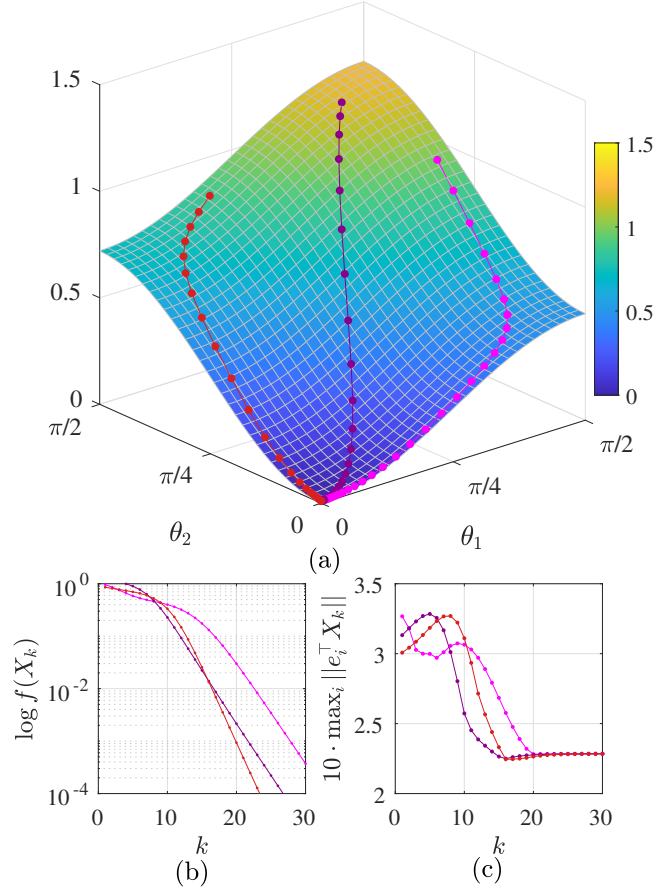


Figure 6: (a) Illustration of trajectories of Riemannian gradient descents on f_{full} . We choose the ground truth matrix to be a 100×200 matrix of rank 2. The step-size is fixed $\eta = 0.1$. (b) Objective values along the trajectories in log-scale. (c) The incoherence parameters along the trajectories.

Geometry of related problems. It is natural to ask whether one could characterize similar results for other related problems. In fact, the main observation in Ge et al. (Ge et al., 2017) is that their analysis for matrix completion also applies to other low rank recovery problems like matrix sensing and robust PCA. Based on this, we suspect that similar landscape results could be characterized for these two problems. Another possibility is to study robust subspace recovery (Maunu et al., 2019) in light of Remark 4.

Formulations based on other distances. In Section 3.1, we interpreted (3.2) as a weighted version of the projection distance. Given this interpretation, it would be interesting to see whether matrix completion can be formulated using other notions of distances between subspaces (Edelman et al., 1998, §4.3). Would other distances lead to a better formulation? We note that this question is already partially explored by Dai et al. (2012) where they consider the chordal distance for the purpose of *consistent* matrix completion.

Acknowledgement

We thank Suvrit Sra for stimulating discussions, especially regarding the geodesic convexity results (Lemma 2 and Corollary 5). We thank Tyler Maunu for pointing us to several related works. We thank Sinho Chewi for discussion regarding Remark 3 and also for various comments and suggestions on the manuscript. We thank Chen Lu for critical comments regarding the formulation.

References

- Absil, P.-A., Mahony, R., and Sepulchre, R. (2004). Riemannian geometry of Grassmann manifolds with a view on algorithmic computation. *Acta Applicandae Mathematica*, 80(2):199–220.
- Bai, Y., Jiang, Q., and Sun, J. (2018). Subgradient descent learns orthogonal dictionaries. *arXiv preprint arXiv:1810.10702*.
- Balzano, L., Nowak, R., and Recht, B. (2010). Online identification and tracking of subspaces from highly incomplete information. In *2010 48th Annual allerton conference on communication, control, and computing (Allerton)*, pages 704–711. IEEE.
- Bhojanapalli, S., Neyshabur, B., and Srebro, N. (2016). Global optimality of local search for low rank matrix recovery. *Advances in Neural Information Processing Systems*, 29:3873–3881.
- Bohorquez, C. O., Khoo, Y., and Ying, L. (2020). Maximizing robustness of point-set registration by leveraging non-convexity. *arXiv preprint arXiv:2004.08772*.
- Boumal, N. (2020). An introduction to optimization on smooth manifolds. Available online.

- Boumal, N. and Absil, P.-a. (2011). RTRMC: a Riemannian trust-region method for low-rank matrix completion. In *Advances in neural information processing systems*, pages 406–414.
- Boumal, N. and Absil, P.-A. (2015). Low-rank matrix completion via preconditioned optimization on the Grassmann manifold. *Linear Algebra and its Applications*, 475:200–239.
- Burer, S. and Monteiro, R. D. (2003). A nonlinear programming algorithm for solving semidefinite programs via low-rank factorization. *Mathematical Programming*, 95(2):329–357.
- Cambier, L. and Absil, P.-A. (2016). Robust low-rank matrix completion by Riemannian optimization. *SIAM Journal on Scientific Computing*, 38(5):S440–S460.
- Candès, E. and Recht, B. (2012). Exact matrix completion via convex optimization. *Commun. ACM*, 55(6):111–119.
- Candès, E. J. and Recht, B. (2009). Exact matrix completion via convex optimization. *Foundations of Computational mathematics*, 9(6):717.
- Chen, Y. and Wainwright, M. J. (2015). Fast low-rank estimation by projected gradient descent: General statistical and algorithmic guarantees. *arXiv preprint arXiv:1509.03025*.
- Dai, W., Kerman, E., and Milenkovic, O. (2012). A geometric approach to low-rank matrix completion. *IEEE Transactions on Information Theory*, 58(1):237–247.
- Dai, W., Milenkovic, O., and Kerman, E. (2011). Subspace evolution and transfer (SET) for low-rank matrix completion. *IEEE Transactions on Signal Processing*, 59(7):3120–3132.
- De Sa, C., Re, C., and Olukotun, K. (2015). Global convergence of stochastic gradient descent for some non-convex matrix problems. In *International Conference on Machine Learning*, pages 2332–2341. PMLR.
- Edelman, A., Arias, T. A., and Smith, S. T. (1998). The geometry of algorithms with orthogonality constraints. *SIAM journal on Matrix Analysis and Applications*, 20(2):303–353.
- Ge, R., Jin, C., and Zheng, Y. (2017). No spurious local minima in nonconvex low rank problems: a unified geometric analysis. In *Proceedings of the 34th International Conference on Machine Learning-Volume 70*, pages 1233–1242.
- Ge, R., Lee, J. D., and Ma, T. (2016). Matrix completion has no spurious local minimum. *Advances in Neural Information Processing Systems*, 29:2973–2981.
- Grassmann, H. (1862). *Die Ausdehnungslehre*. Enslin, Germany.
- Hardt, M. (2014). Understanding alternating minimization for matrix completion. In *2014 IEEE 55th Annual Symposium on Foundations of Computer Science*, pages 651–660. IEEE.

- Hardt, M. and Wootters, M. (2014). Fast matrix completion without the condition number. In *Conference on learning theory*, pages 638–678.
- Hou, T. Y., Li, Z., and Zhang, Z. (2020). Fast global convergence for low-rank matrix recovery via Riemannian gradient descent with random initialization. *arXiv preprint arXiv:2012.15467*.
- Jain, P., Netrapalli, P., and Sanghavi, S. (2013). Low-rank matrix completion using alternating minimization. In *Proceedings of the forty-fifth annual ACM symposium on Theory of computing*, pages 665–674.
- Jordan, C. (1875). Essai sur la géométrie à n dimensions. *Bulletin de la Société mathématique de France*, 3:103–174.
- Keshavan, R. H., Montanari, A., and Oh, S. (2010). Matrix completion from a few entries. *IEEE transactions on information theory*, 56(6):2980–2998.
- Keshavan, R. H. and Oh, S. (2009). A gradient descent algorithm on the grassman manifold for matrix completion. *arXiv preprint arXiv:0910.5260*.
- Klingenberg, W. (1959). Contributions to riemannian geometry in the large. *Annals of Mathematics*, pages 654–666.
- Koren, Y. (2009). The bellkor solution to the netflix grand prize. *Netflix prize documentation*, 81(2009):1–10.
- Li, X., Chen, S., Deng, Z., Qu, Q., Zhu, Z., and So, A. M. C. (2019). Weakly convex optimization over stiefel manifold using Riemannian subgradient-type methods. *arXiv*, pages arXiv–1911.
- Maunu, T., Zhang, T., and Lerman, G. (2019). A well-tempered landscape for non-convex robust subspace recovery. *J. Mach. Learn. Res.*, 20(37):1–59.
- Miao, J. and Ben-Israel, A. (1992). On principal angles between subspaces in \mathbb{R}^n . *Linear Algebra Appl*, 171(92):81–98.
- Mishra, B., Apuroop, K. A., and Sepulchre, R. (2012). A Riemannian geometry for low-rank matrix completion. *arXiv preprint arXiv:1211.1550*.
- Mishra, B., Meyer, G., Bonnabel, S., and Sepulchre, R. (2014). Fixed-rank matrix factorizations and Riemannian low-rank optimization. *Computational Statistics*, 29(3-4):591–621.
- Ngo, T. and Saad, Y. (2012). Scaled gradients on Grassmann manifolds for matrix completion. *Advances in neural information processing systems*, 25:1412–1420.
- Park, D., Kyrillidis, A., Carmanis, C., and Sanghavi, S. (2017). Non-square matrix sensing without spurious local minima via the burer-monteiro approach. In *Artificial Intelligence and Statistics*, pages 65–74. PMLR.

- Pitaval, R.-A., Dai, W., and Tirkkonen, O. (2015). Convergence of gradient descent for low-rank matrix approximation. *IEEE Transactions on Information Theory*, 61(8):4451–4457.
- Simonsson, L. and Eldén, L. (2010). Grassmann algorithms for low rank approximation of matrices with missing values. *BIT Numerical Mathematics*, 50(1):173–191.
- Sun, J., Qu, Q., and Wright, J. (2016). Complete dictionary recovery over the sphere i: Overview and the geometric picture. *IEEE Transactions on Information Theory*, 63(2):853–884.
- Sun, R. and Luo, Z.-Q. (2016). Guaranteed matrix completion via non-convex factorization. *IEEE Transactions on Information Theory*, 62(11):6535–6579.
- Vandereycken, B. (2013). Low-rank matrix completion by Riemannian optimization. *SIAM Journal on Optimization*, 23(2):1214–1236.
- Wei, K., Cai, J.-F., Chan, T. F., and Leung, S. (2016). Guarantees of Riemannian optimization for low rank matrix recovery. *SIAM Journal on Matrix Analysis and Applications*, 37(3):1198–1222.
- Wong, Y.-C. (1967). Differential geometry of Grassmann manifolds. *Proceedings of the National Academy of Sciences of the United States of America*, 57(3):589.
- Wong, Y.-C. (1968). Sectional curvatures of grassmann manifolds. *Proceedings of the National Academy of Sciences of the United States of America*, 60(1):75.
- Zhao, T., Wang, Z., and Liu, H. (2015). A nonconvex optimization framework for low rank matrix estimation. *Advances in Neural Information Processing Systems*, 28:559–567.
- Zhu, Z., Ding, T., Robinson, D., Tsakiris, M., and Vidal, R. (2019). A linearly convergent method for non-smooth non-convex optimization on the Grassmannian with applications to robust subspace and dictionary learning. In *Advances in Neural Information Processing Systems*, pages 9442–9452.